Journal of Organometallic Chemistry 891 (2019) 12–19

Contents lists available at ScienceDirect

Journal of Organometallic Chemistry

journal homepage: www.elsevier.com/locate/jorganchem

# Modulation of the solubility properties of arene ruthenium complexes bearing stannyl ligands as potential anti-cancer agents

Clara Berg [a], Suviti Chari [a], Kaste Jurgaityte [a], Alice Laurora [a], Mateusz Naldony [a], Frances Pope [a], Dario Romano [b, c], Thato Medupe [d], Sharon Prince [e], Siyabonga Ngubane [d, **], Judith Baumgartner [f], Burgert Blom [a, *]

[a] Maastricht Science Programme, Faculty of Science and Engineering, Maastricht University, Kapoenstraat 2, PO Box 616, 6200 MD, Maastricht, the Netherlands
[b] Department of Biobased Materials, Faculty of Science and Engineering, Maastricht University, Brightlands Chemelot Campus, Urmonderbaan 22, Geleen, 6167 RD, the Netherlands
[c] Aachen-Maastricht Institute of Biobased Materials, Brightlands Chemelot Campus, Urmonderbaan 22, Geleen, 6167 RD, the Netherlands
[d] University of Cape Town, Department of Chemistry, Rondebosch 7701, Cape Town, South Africa
[e] University of Cape Town, Department of Human Biology, Observatory 7935, Cape Town, South Africa
[f] Institut für Anorganische Chemie, Technische Universität Graz, Stremayrgasse 9, A-8010 Graz, Austria

ARTICLE INFO

*Article history:*
Received 23 January 2019
Received in revised form
2 April 2019
Accepted 3 April 2019
Available online 8 April 2019

*Keywords:*
Ruthenium
Solubility
Stannyl ligands
Arene
Anti-cancer
MCF-7 human breast adenocarcinoma cells

ABSTRACT

Cleavage of the known ruthenium dimer $[RuCl_2(\eta^6\text{-}C_6H_5OCH_2CH_2OH)]_2$ (**1**), bearing a hydrophilic substituent on the $\eta^6$ coordinated aromatic ring, with the phosphine ligands: triphenyl phosphine, triphenyl phosphite, trimethyl phosphite, and 1,3,5-triaza-7-phosphaadamantane (PTA) afforded the known complexes $[RuCl_2(\eta^6\text{-}C_6H_5OCH_2CH_2OH)(PPh_3)]$ (**2a**), $[RuCl_2(\eta^6\text{-}C_6H_5OCH_2CH_2OH)\{P(OPh)_3\}]$ (**2b**), $[RuCl_2(\eta^6\text{-}C_6H_5OCH_2CH_2OH)\{P(OMe_3)\}]$ (**2c**), and $[RuCl_2(\eta^6\text{-}C_6H_5OCH_2CH_2OH)(PTA)]$ (**4**). The reaction of the known complex **2a** with $SnCl_2$ afforded, by facile insertion of the $SnCl_2$ moiety into the Ru–Cl bond, the novel complex $[RuCl(\eta^6\text{-}C_6H_5OCH_2CH_2OH)(PPh_3)(SnCl_3)]$ (**3a**). Similarly, the reaction of complex **2b** with $SnCl_2$ afforded the novel complex $[RuCl(\eta^6\text{-}C_6H_5OCH_2CH_2OH)\{P(OPh)_3\}(SnCl_3)]$ (**3b**). Complexes **3a** and **3b** were fully characterized by spectroscopy (Infrared (IR) -spectroscopy, $^1H$, $^{31}P$ and $^{119}Sn$ Nuclear Magnetic Resonance (NMR) spectroscopy, UV–Vis spectroscopy and high resolution ESI-MS) and their thermal behaviour elucidated by Thermogravimetric Analysis (TGA). Density Functional Theory (DFT) calculations (Level of theory B3LYP, basis set for H, C, P, O, N and Cl is 6-31 + G (d,p) and for Ru and Sn is DGDZVP) for complex **3a**, **3b** and **4** were also carried out, in particular to elucidate the bonding situation between Ru and Sn in complexes. The hitherto unprecedented anti-cancer activity of the complexes **2a** – **2c** as well as the novel stannyl complexes **3a** and **3b** were evaluated against MCF-7 (oestrogen receptor positive) human breast adenocarcinoma cell lines. All complexes show activity active against MCF-7 cell lines, indicating potential application as an anti-tumor agent.



## 1. Introduction

Cis-diamminedichloridoplatinum (II), commonly known as cisplatin, is administered intravenously to treat patients suffering from numerous types of cancers including testicular, cervical and certain lung cancers [1,2]. In an attempt to increase the bioavailability and limit the side-effects of chemotherapeutic drugs, ruthenium complexes have been investigated as an alternative to platinum [3–8]. A detailed mechanistic study of the complex [Ru(*p*-cymene)(NHC)$Cl_2$] (NHC = 1,3-bis(4-(*tert*-butyl)benzylimidazol-2-ylidene), has been reported and shows antiproliferate activity of EC109 cells is accompanied by up-regulation of p53 and p21 proteins and a down-regulation of cyclin D1 [9]. The aforementioned proteins are involved in the cell cycle, which can cause cell death if not properly regulated [9]. Ruthenium has potentially important pharmacological advantages, including its access to a range of oxidation states (II, III and IV) [6]. The energy barriers between each

* Corresponding author.
** Corresponding author.
*E-mail addresses:* siyabonga.ngubane@uct.ac.za (S. Ngubane), burgert.blom@maastrichtuniversity.nl (B. Blom).

https://doi.org/10.1016/j.jorganchem.2019.04.002
0022-328X/

state are relatively low, allowing a change in oxidation state under relevant physiological conditions when inside the cell [6]. Despite the flexible oxidation states, ligand exchange rates in water are relatively slow and correlate with the time-scale of cellular reproduction [10]. If a ruthenium ion binds to a biomolecular target in the cell, it will most likely remain bound for the remainder of that cell's lifetime, which can be crucial for cytotoxic activity [10]. Research has been done on the cytotoxic activity of ruthenium arene complexes, giving promising results [3,8]. One such example is RAPTA-C (Fig. 1) [11–13]. This piano-stool ruthenium arene complex bears a 1,3,5-triaza-7-phosphaadamantane ligand and presents promise, similar to the drug NAMI-A, another active agent (Fig. 1) [14,15]. Interesting chlorambucil derivatives of RAPTA-C have also been reported more recently in the literature [13].

Previous work has shown that tin groups possess cytotoxic properties [16], and the effectiveness of a tin dichloride ($SnCl_2$) insertion on ruthenium arene complexes facilitates an improvement in cytotoxicity [17]. In this vein, we have recently reported neutral complexes of the type [RuCl($\eta^6$-$C_6H_6$)($PR_3$)($SnCl_3$)] (R = OPh, Ph, OMe), the ionic complexes [Ru($\eta^6$-$C_6H_6$)($PPh_3$)($SnCl_3$)(DMAP)]$^+BF_4^-$ and [(RuCl($\eta^6$-$C_6H_6$)($PPh_3$)(DMAP)]$^+BF_4^-$; the latter exhibit promising cytotoxic activity towards the cell lines A2780 (human ovarian cancer) and A2780cisR (human ovarian cisplatin-resistant cancer) (Fig. 2) [18]. In particular, [Ru($\eta^6$-$C_6H_6$)($PPh_3$)($SnCl_3$)(DMAP)]$^+BF_4^-$ exhibits some cancer cell selectivity. The neutral complexes [RuCl($\eta^6$-$C_6H_6$)($PR_3$)($SnCl_3$)] were shown to be less cytotoxic and exhibited in some cases low cytotoxicity. In a further study, complexes of the type [RuCl($\eta^6$-Arene)($PR_3$)($GeCl_3$)] were shown to exhibit very low cytotoxicity towards A2780 which we proposed was linked to the rapid aquation of the complexes [19]. Possibly, the lower than expected cytotoxicity in the complexes [RuCl($\eta^6$-$C_6H_6$)($PR_3$)($SnCl_3$)] could be linked to the their extreme insolubility in aqueous or non-polar media. Hence, solubility in aqueous media seemed to play a distinctive role in the cytotoxic activity: very insoluble complexes exhibited low activity, despite having $SnCl_3$ groups which could be expected to enhance cytotoxicity [18]. Inspired by these findings, and as part of our ongoing investigation into elucidating the effect of incorporating a stannyl group into the ligand sphere of a Ru (II) arene complex and its effect on cytotoxicity and cancer cell selectivity, we synthesized a series of both known and novel complexes of the type [RuClX($\eta^6$-$C_6H_5OCH_2CH_2OH$)($PR_3$)] (X = Cl or $SnCl_3$, R = OMe, Ph, OPh). These complexes bear a hydrophilic tail on the arene moiety, which might enhance solubility in aqueous media. The cytotoxicity towards MCF-7 (oestrogen receptor positive) human breast adenocarcinoma cells is reported here. Compounds are benchmarked against the cisplatin clinical drug (CDDP).

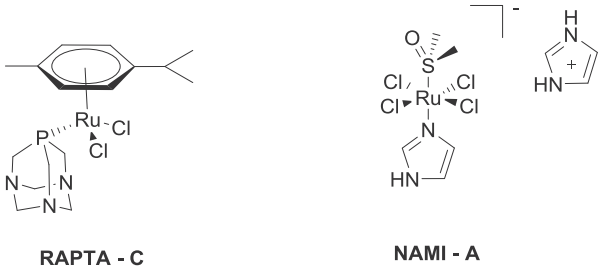


**Fig. 1.** The drug candidates RAPTA-C and NAMI-A are undergoing clinical trials for the treatment of secondary tumors [11,14].

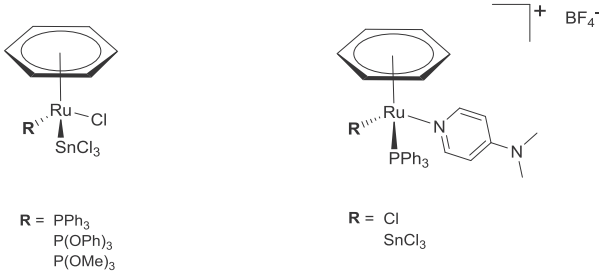


**Fig. 2.** Ruthenium arene complexes exhibiting promising cytotoxic activity towards the cell lines A2780 (human ovarian cancer) and A2780cisR (human ovarian cisplatin-resistant cancer) [18].

## 2. Results and discussion

### 2.1. Synthesis of the complexes

The precursor selected for this synthesis is the easily accessible ruthenium dimer [$RuCl_2(\eta^6$- $C_6H_5OCH_2CH_2OH)]_2$ (**1**) [20], which enables facile entry to the known piano-stool complexes **2a**, **2b** and **2c** through simple ligand cleavage reactions with the appropriate phosphine (Scheme 1) [20,21]. For the synthesis of the known complexes **2a** and **2b** a modified procedure from Lastra-Barreira et al. was used [20]. Amendments were made by stirring the solution for an extended time period and eliminating the necessity of column chromatography to afford a simplified procedure with a higher overall yield (77.9% and 91.0% respectively). Subsequent reaction of complexes **2a** and **2b** with $SnCl_2$ affords the novel complexes [RuCl($\eta^6$-$C_6H_5OCH_2CH_2OH$)($PPh_3$)($SnCl_3$)](**3a**) and [RuCl($\eta^6$-$C_6H_5OCH_2CH_2OH$){$P(OPh)_3$}($SnCl_3$)](**3b**) respectively by insertion of $SnCl_2$ into the Ru–Cl bond. An analogous complex to RAPTA-C was synthesized utilizing a PTA ligand, affording the known complex **4**.

### 2.2. Spectroscopic characterization of the novel complexes

#### 2.2.1. [RuCl($\eta^6$-$C_6H_5OCH_2CH_2OH$)($PPh_3$)($SnCl_3$)] (*3a*)

A downfield shift of 3 ppm can be observed in the $^{31}P\{^1H\}$ NMR spectrum of complex **3a** in comparison to the precursor **2a**. This is in close analogy to our earlier observations, however, in contrast to our earlier findings [18], no $^{119}Sn$ or $^{117}Sn$ satellites were observed. Due to the insertion of $SnCl_2$ into the Ru–Cl bond of the precursor, the Ru center is rendered chiral and this results in loss of symmetry of the arene ring: in the $^1H$ NMR spectrum several resonance signals are observed corresponding to the asymmetric nature of the arene ring. This is also in close analogy to our earlier reported findings [18,19]. Indeed, starting from the achiral precursor, **2a,** the insertion of $SnCl_2$ induces a chiral center at Ru which should afford a racemic mixture of both enantiomers (***rac*-3a**). This would be expected to afford one set of resonance signals in all NMR spectra (we represent, for simplicity in all our schemes, one of these stereoisomers for **3a** and **3b**). The IR spectrum of **3a** shows a very weak and broad stretching vibration at 3078 $cm^{-1}$, which confirms the presence of the OH group. TGA shows an onset of 3.84% (29.26 g/mol) at 75 °C which may be due to trace impurities. The greatest mass loss of 14.22% (108.35 g/mol) occurred at the thermal event at temperatures in the range 321.01–342.26 °C. The weight of the leftover sample at the temperature of 493.45 °C corresponded to 44.40% (339.30 g/mol) which could be attributed to the Ru metal center and Sn. The observed decomposition point at 205 °C is in accordance with the thermal event in the range 128–237 °C. The high resolution mass spectrum (ESI) of the complex shows a complex fragmentation pattern, with the base peak corresponding to the loss of the trichlorostannyl ligand from the parent ion i.e. $[M - SnCl_3]^+$. This suggests that the stannyl ligand is somewhat weakly bound to the metal center, which is supported by our DFT

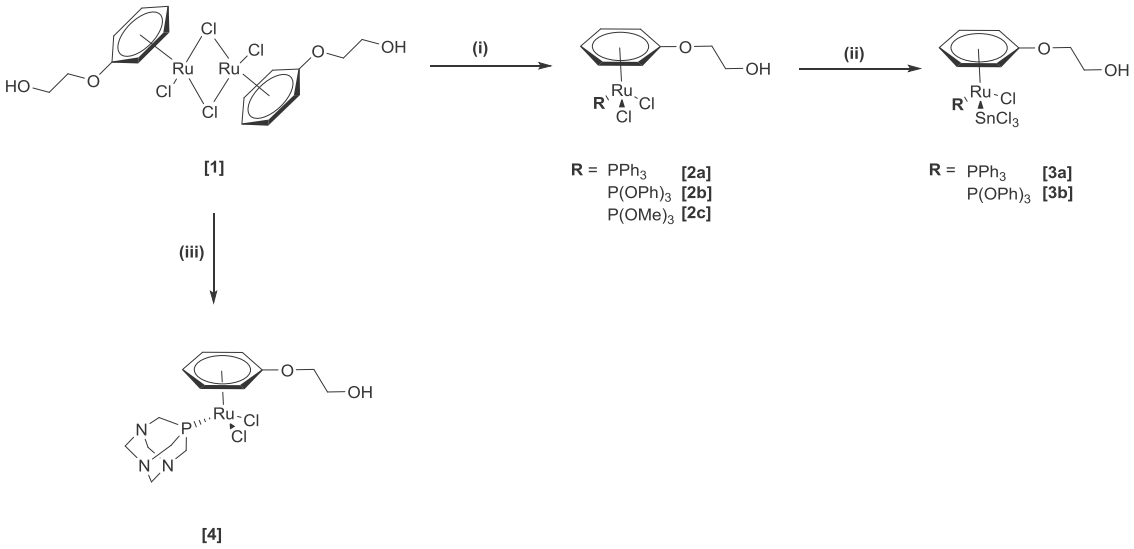


**Scheme 1.** Overview of complexes synthesized in this study. (i) 2 equiv. $PPh_3$/$P(OPh)_3$/$P(OMe)_3$ in DCM, r.t., 17 h; (ii) 1 equiv. $SnCl_2$ in DCM, reflux, 4.5 h; (iii) 2 equiv. PTA in DCM: methanol (1:1), 50 °C, 30 min.

calculations showing a Wiberg Bond Index of 0.723 (see below). This fragmentation is in analogy to our previously reported analogous germyl complexes [19].

### 2.2.2. *[RuCl($\eta^6$-$C_6H_5OCH_2CH_2OH$){P(OPh)$_3$}($SnCl_3$)] (**3b**)*

The chirality at the ruthenium center results in different environments for each proton on the arene ring visible in the $^1$H NMR spectrum in analogy to **3a**. The OH group can be assigned to a distinct doublet of doublets at $\delta = 4.52$ ppm. This is a result of the adjacent diastereotopic $CH_2$ hydrogens which appear to be in distinct environments. The $OCH_2$ attached to the arene ring appears as an unresolved broad peak ($\delta = 3.93–3.83$ ppm) as a result of complex $^3J$ coupling to each of the diastereotopic H atoms on the adjacent $CH_2$. When comparing the resonance signal in the $^{31}P\{^1H\}$ NMR to the precursor **2b** a downfield shift (by 7.3 ppm) upon the tin insertion is found. This is comparable to what is observed for complex **3a** and its precursor **2a** and our earlier findings [18]. In the $^{119}Sn$ $\{^1H\}$ NMR spectrum of **3b** a doublet resonance signal is observed at $\delta = -169.3$ ppm confirming the attachment of the $SnCl_3$ moiety to the Ru (II) center, as the doublet arises from a $^2J_{Sn,P}$ coupling. This confirms additionally, that also in solution, no fluxional process is occurring, and the $SnCl_3$ is statically bound to the Ru center, as any decomplexation equilibrium would quench the coupling to P (Fig. 3). In close analogy to **3a**, complex **3b** exhibits a high resolution mass spectrum (ESI) which has a complex fragmentation pattern, with one of the high intensity signals corresponding to the loss of $SnCl_3$ from the parent ion.

In the IR spectrum recorded for this sample a very weak and

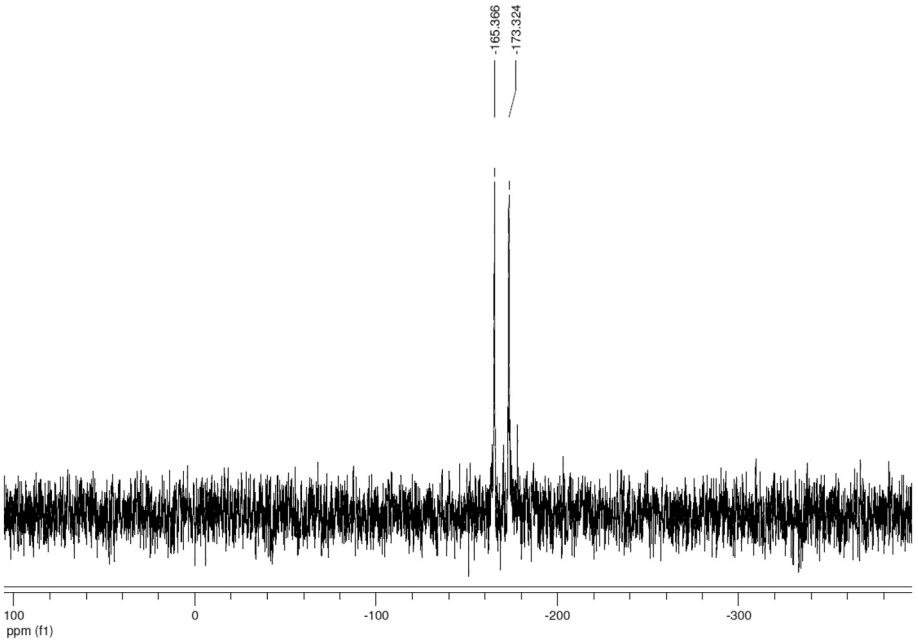


**Fig. 3.** $^{119}Sn$ NMR spectrum of complex **3b**.

broad peak at 3000 $cm^{-1}$ denotes the presence of the OH group as in complex **3a**. The analysis using UV–Vis spectroscopy shows the highest absorbance at the $\lambda_{max} = 452$ nm. When compared to the precursor **2b**, a blue shift of 30 nm has been observed, which is in agreement with the visible colour change. The TGA analysis of complex **3b** reveals the initial mass loss of 3.27% (26.50 g/mol) at a temperature of 135 °C. The biggest mass decrease of 18.40% (149.00 g/mol) was recorded at the thermal event at temperatures in the range 225.24–339.11 °C.

### 2.2.3. Water solubility

By the addition of a hydrophilic substituent on the arene ligand an improved water solubility of the complexes was intended. Simple tests were conducted to assess the relative water solubilities of the complexes. Complexes **3a** and **4** were found to be somewhat water soluble at 20 °C (0.03 mg/mL and 10 mg/mL respectively). However, **2b** and **3b** were found to be insoluble.

### 2.2.4. Single crystal X-Ray investigation of *3b*

Crystals, suitable for single crystal X-ray diffraction analysis, of complex **3b** were obtained by slow evaporation of a dilute sample of **3b** in dichloromethane at 7 °C (Fig. 4), providing additional evidence of $SnCl_2$ insertion into the Ru–Cl bond of its precursor **2b**. Complex **3b** has features typical of piano-stool Ru(II) arene complexes of this type (see Ref. [18] and references therein). Complex **3b** features a Ru–Sn bond length of 2.5627 (19) Å, which is comparable to the complex [($\eta^6$-$C_6H_6$)RuCl($SnCl_3$)(P($OPh)_3$)] (2.5686 Å) reported by us earlier [18]. The complex exhibits a slightly distorted tetrahedral geometry about the Sn center evidenced by the slight deviations from a perfect tetrahedral geometry: Cl (1)-Sn(1)-Ru (1) 120.30 (16), Cl (3)-Sn(1)-Ru (1) 118.9 (4), Cl (2)-Sn(1)-Ru (1) 115.34 (17). Similarly, the geometry around the Ru center can be described as distorted tetrahedral.

## 2.3. Cytotoxic testing

The anti-cancer activity of Ru(II) arene complexes (5 & 10 μM prepared in DMSO) on the MCF-7 (oestrogen-receptor positive) human breast adenocarcinoma, was evaluated using the MTT colorimetric assay (Fig. 5) [22]. In all assays, DMSO diluted in free medium was included as a negative control and the clinical drug cisplatin (CDDP) was included as a positive control with an $IC_{50}$ value of 5.47 μM (see Figure S9), comparable to that reported in literature for the same cell-line (5.75 μM) [23]. The % cell viability against the Ru(II) arene complexes is herein reported in Fig. 5. Complexes **2a** – **2c**, **3a** and **4** show activity against the MCF-7 cells, at both concentrations tested with complex **3b** showing low activity. Complex **2b** is the most active (<50% cell survival) at 10 μM which may be attributed to the presence of the triphenyl phosphate ligand. This possibly enhances the solubility of the drug molecule upon direct contact or interaction with the human albumin serum (HSA) protein enabling its transportation to the biologically active target at enhanced rates [24]. Compound **4** is suspected to undergo an aquation reaction in solution to yield its complex cation and the respective counter ion which may account for the observed trend specifically for this compound. The tin compounds **3a** and **3b** exhibit some cytotoxicity as compared with the complexes reported earlier of the type [RuCl($\eta^6$-$C_6H_6$)($PR_3$)($SnCl_3$)] which were largely inactive. This provides some evidence that attachment of the hydrophilic tail increases the water solubility and hence the cytotoxic activity.

Although compound **2b** was insoluble in water, it was soluble in DMSO and is the most active against the MCF-7 cells in this series. Compound **3b** was also insoluble in water and only partially soluble in DMSO and it showed only some activity against the MCF-7 cells. The hydrophobicity of **3b** may be attributed to the presence of the trichlorostannyl ligand coordinated to the ruthenium metal center,

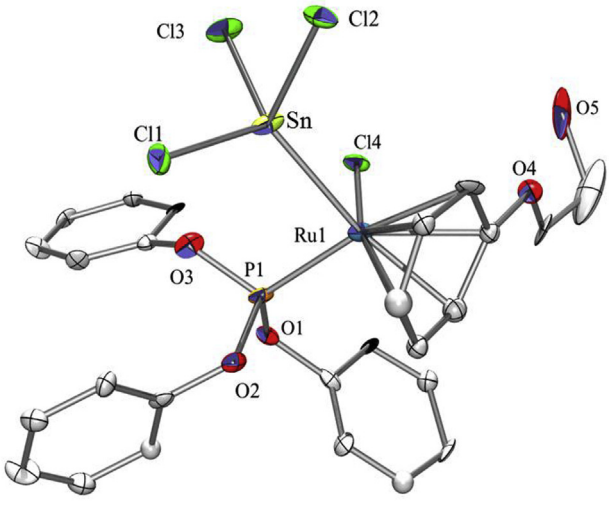


**Fig. 4.** ORTEP representation of the X-ray structure of complex *rac*-**3b** at the 30% probability level. Disorder at Cl3 not represented. Selected bond lengths [Å]: Sn(1)–Ru (1) 2.5627 (19), Cl (3)–Sn(1) 2.409 (9), Sn(1)–Cl (2) 2.351 (5), Sn(1)–Cl (1) 2.377 (7), Ru (1)–P (1) 2.246 (5). Selected bond angles [°]: P (1)-Ru (1)-Sn(1) 86.56 (13), Cl (4)-Ru (1)-Sn(1) 85.46 (14), P (1)-Ru (1)-Cl (4) 85.80 (17), Cl (1)-Sn(1)-Ru (1) 120.30 (16), Cl (3)-Sn(1)-Ru (1) 118.9 (4), Cl (2)-Sn(1)-Ru (1) 115.34 (17). (Other metric parameters found in the supporting information).

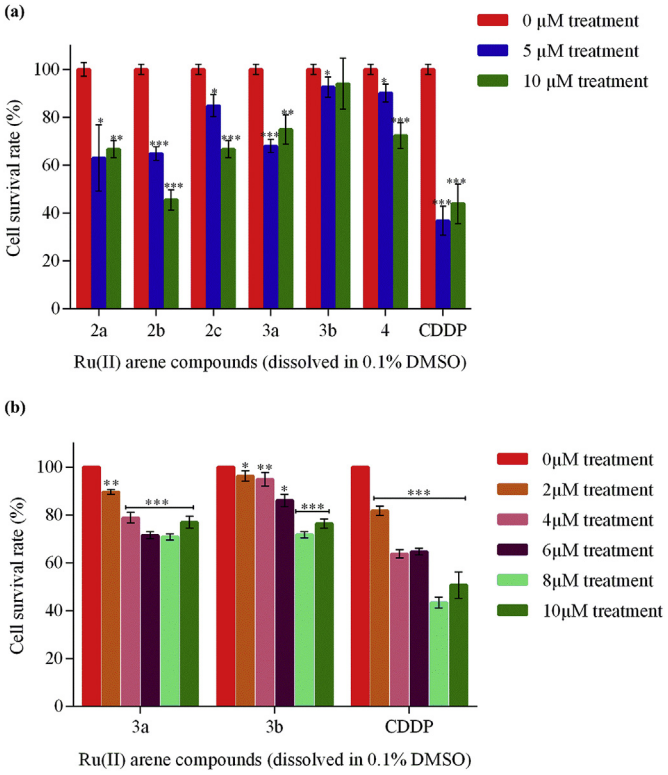


**Fig. 5.** MTT cell viability assays for MCF-7 cells treated for 24 h with Ru arene organometallic complexes **2a-c**, **3a**, **3b** & **4** prepared at (a) 5 & 10 μM and (b) 0–10 μM or vehicle (DMSO) or Cisplatin (CDDP). Graphs show mean cell viability as a percentage of vehicle control ± SEM for each concentration of complexes determined from three independent experiments performed in quadruplicate [*p < 0.5; **p < 0.01; ***p < 0.001].

impeding the solubility of the compound in DMSO. This phenomenon was also observed and reported for the half-sandwich ruthenium complex, $[(\eta^6\text{-}C_6H_6)Ru(SnCl_3)_2(P(OMe)_3)]$, bearing two trichloro stannyl ligand moieties [18], for which the antiproliferative activity was measured against ovarian cancer cells after 72 h of continuous drug action.

In the present study, the compound was used after centrifugation of the stock solution to help aid solubility before dilution with the supplemented RPMI medium. Complexes **2a, 3a** and **3b** at 10 μM indicate an increase in the cell viability, possibly due to the uptake limit of the complexes. A multi-dose cell viability of compounds **3a** and **3b** is shown in Fig. 5b indicating an approximate cell death of 30% at 8 μM, beyond which an increase in the cell viability is observed.

### 2.4. Density functional calculations

The optimized structures of complexes **3a**, **3b** and **4** are shown in Fig. 6.

In all the optimized structures, the Ru atoms show pseudo-tetrahedral geometry. For complexes **3a** and **3b**, the Sn atoms also show pseudo-tetrahedral geometry; in addition, the optimized structures of **3a** and **3b** are very similar in the arene and $SnCl_3$ moieties. A visual representation of the highest occupied energy orbitals (HOMO) for complexes **3a**, **3b** and **4** can be found in Fig. 7; while a visual representation of the lowest unoccupied energy orbitals (LUMO) is depicted in Fig. 8.

For complex **3b**, the DFT-optimized structure matches the crystallographic structure obtained by X-ray analysis within 8% difference according to selected values of bond length and angles reported in Table 1.

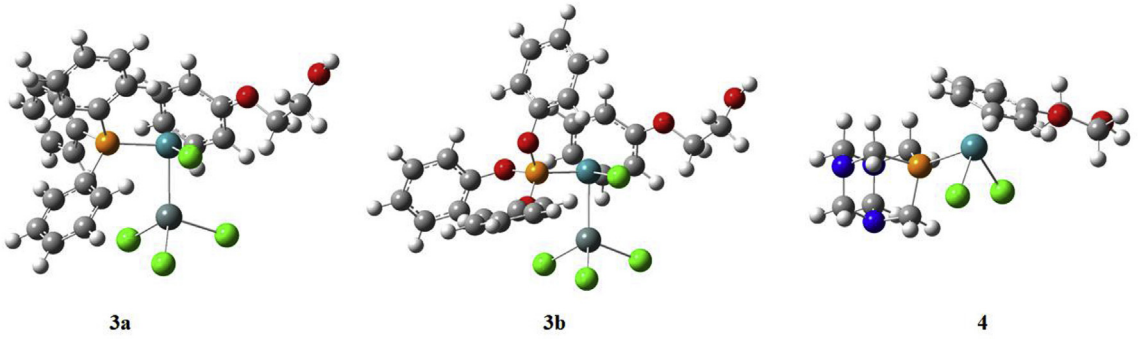


**Fig. 6.** Density Functional Theory optimized structures for complexes **3a** (left), **3b** (middle) and **4** (right). Level of theory B3LYP, basis set for H, C, P, O, N and Cl is 6-31 + G (d,p) and for Ru and Sn is DGDZVP.

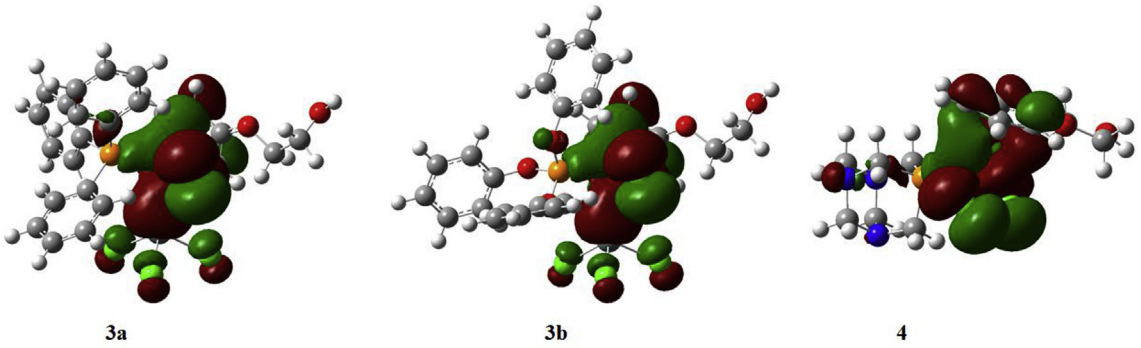


**Fig. 7.** Graphical representation of the highest occupied energy orbitals (HOMO) for complexes **3a** (left), **3b** (middle) and **4** (right). Level of theory B3LYP, basis set for H, C, P, O, N and Cl is 6-31 + G (d,p) and for Ru and Sn is DGDZVP.

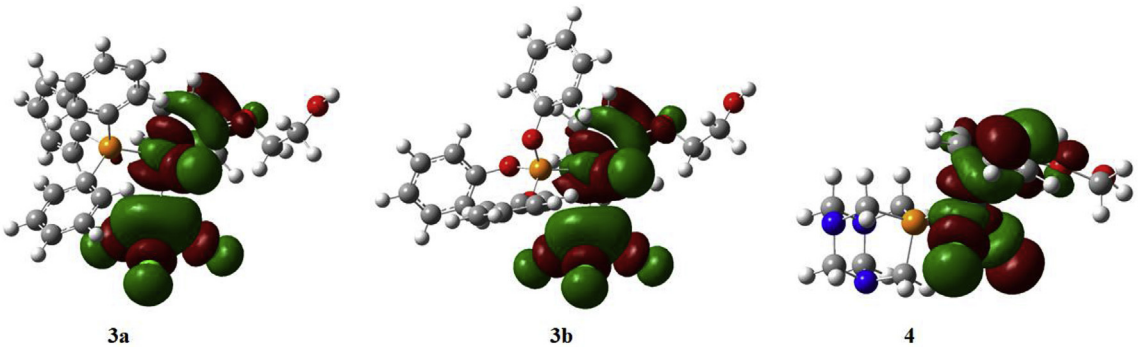


**Fig. 8.** Graphical representation of the lowest unoccupied energy orbitals (LUMO) for complexes **3a** (left), **3b** (middle) and **4** (right). Level of theory B3LYP, basis set for H, C, P, O, N and Cl is 6-31 + G (d,p) and for Ru and Sn is DGDZVP.

**Table 1**
Comparison of the DFT-optimized structure and the X-ray crystallographic data.

| | X-Ray | | DFT optimized | | Difference (%) |
|---|---|---|---|---|---|
| | Bond Lengths [Å] | Angles Angles [°] | Bond Lengths [Å] | Angles Angles [°] | |
| Sn1–Cl1 | 2.377 | | 2.432 | | 2 |
| Sn1–Cl2 | 2.351 | | 2.434 | | 3 |
| Sn1–Cl3 | 2.409 | | 2.384 | | −1 |
| Sn1–Ru1 | 2.563 | | 2.638 | | 3 |
| Ru1–Cl4 | 2.379 | | 2.447 | | 3 |
| Ru1–P1 | 2.246 | | 2.276 | | 1 |
| Ru1–Sn1–Cl4 | | 85.46 | | 85.47 | 0 |
| Ru1–Sn1–P1 | | 86.56 | | 88.77 | 2 |
| Cl1–Sn1–Cl2 | | 96.30 | | 99.34 | 3 |
| Cl1–Sn1–Cl3 | | 108.00 | | 101.86 | −6 |
| Cl2–Sn1–Cl3 | | 92.50 | | 100.77 | 8 |

For complexes **3a** and **3b**, the HOMO is mainly located on the Ru–Sn bond and the Ru and Cl atoms. This indicates that the oxygen atoms connected to the phosphorous do not significantly influence the HOMO of complex **3b** with respect to complex **3a**. For complex **4**, the HOMO is mainly located on the Cl atoms and along the Ru-arene coordination.

For complexes **3a** and **3b** the LUMO is mainly located on the Sn–Cl bonds as well as on the Ru, Ru–Cl bond and delocalized over the arene. Likewise, the analysis of the HOMOs, the LUMOs of the optimized structures for **3a** and **3b** are very similar, denoting a negligible effect of the oxygens bound to the phosphorous on the LUMO. Similar results are obtained for the LUMO of complex **4** where the LUMO is located on the Ru–Cl bonds and delocalized on the arene. Natural bond analysis (NBO) was performed to establish the nature of bonds with particular focus on the ruthenium-tin bonds and atoms of complexes **3a** and **3b**. Table 2 summarizes the DFT results of the natural bond order analysis for complexes **3a** and **3b**.

The calculation results show no significant differences between the bond polarizations and the contributions of the different atomic orbitals of Ru and Sn of complexes **3a** and **3b**. Complex **3b** shows a slightly more negative Mulliken charge on the Ru atom most likely due to an increased electron density generated by the presence of the oxygen atoms directly connected to the P atoms coordinated to the Ru center. The Wiberg bond index for the Ru–Sn bond is 0.723 for Complex **3a** and 0.711 for complex **3b**, which is in close agreement with our earlier reported findings for a series of analogous Germyl complexes [19].

## 3. Experimental section

### 3.1. Materials and methods

All reactions were carried out under nitrogen overpressure. Analysis of all complexes proceeded in air as the complexes were air and moisture stable. All commercially available chemicals used were obtained from Sigma-Aldrich and used without further purification. Dimer **1** was prepared according to Soleimannejad et al. [25]. Complex **2c** was prepared following a published procedure from Lastra-Barreira et al. [20]. For complexes **2a** and **2b** the same procedure was used with only minor amendments. Complex **4** was prepared using a procedure reported by Matsina et al. [21]. NMR spectra were recorded on a Bruker Ultrashield 300 or in the case of $^{119}$Sn NMR (111.8 $MH_z$): a Varian Unity INOVA 300 spectrometer. IR spectra were recorded on a Shimadzu MIRacle IR (ATR), UV–Vis on a Shimadzu UV 3600, and TGA spectra were recorded on a TGA Q-500 at the University of Maastricht Brightlands Chemelot Campus, Netherlands. The NMR signals are reported with reference to their solvent residual signals. The peaks in the IR spectra were reported according to their relative intensities: s: strong; w: weak; m: medium; vs: very strong; vw: very weak. The high resolution ESI-MS of **3a** and **3b** was recorded at the University of Stellenbosch Central Anlytical Facilities on a Waters Synapt G2 spectrometer with a cone voltage of 15 V.

X-ray structure determination: For X-ray structure analyses the crystals were mounted onto the tip of glass fibers, and data collection was performed with a BRUKER-AXS SMART APEX CCD diffractometer using graphite-monochromated Mo Kα radiation (0.71073 Å). The data were reduced to $F^2_0$ and corrected for absorption effects with SAINT [26] and SADABS [27,28], respectively. Structures were solved by direct methods and refined by full-matrix least-squares method (SHELXL97 and SHELX2013) [29,30]. All non-hydrogen atoms were refined with anisotropic displacement parameters. Hydrogen atoms were placed in calculated positions to correspond to standard bond lengths and angles. All diagrams were drawn with 30% probability thermal ellipsoids and all hydrogen atoms were omitted for clarity.

Crystallographic data for the structure of compounds **3b** reported in this paper has been deposited with the Cambridge Crystallographic Data Center as supplementary publication no. CCDC 1585436 (**3b**). Copies of data can be obtained free of charge at: http://www.ccdc.cam.ac.uk/products/csd/request/. Figures of solid state molecular structures were generated using Ortep-3 as implemented in WINGX [31] and rendered using POV-Ray 3.6 [32].

**Table 2**
Natural bond analysis calculation for complexes **3a** and **3b**.

| Atom | Bond Polariz. (%) | s-character (%) | p-character (%) | d-character (%) | Mulliken Charge | Wiberg Bond Index |
|---|---|---|---|---|---|---|
| **Complex 3a** | | | | | | |
| **Ru** | 50.47 | 23.52 | 27.73 | 48.75 | −0.709 | 0.723 |
| **Sn** | 49.53 | 82.12 | 17.51 | 0.37 | 0.602 | |
| **Complex 3b** | | | | | | |
| **Ru** | 52.62 | 22.87 | 25.93 | 51.20 | −0.895 | 0.711 |
| **Sn** | 47.38 | 80.27 | 19.32 | 0.41 | 0.648 | |

### 3.2. Cell culture

RPMI 1640 medium (Highveld Biological, Lyndhurst, UK) was used to maintain the human breast adenocarcinoma MCF-7 (oestrogen receptor positive) cell line. The medium was supplemented with 10% Foetal Bovine Serum (FBS), 100 U/ml penicillin and 100 μg/mL streptomycin. Cells were maintained at 37 °C in a 5% $CO_2$-95% air-humidified incubator.

### 3.3. In vitro cytotoxicity evaluation-MTT assay protocol

The complex solutions were prepared by dissolving compounds in DMSO to give 10 mM stock solutions which were used on the same day of treatment. MCF-7 cells were seeded in 96 well plates at a density of $4.5 \times 10^3$ cells per well. After 48 h, cells were treated for 24 h with medium (200 μL) containing the test compounds (0, 5 and 10 μM) or vehicle (10 μM DMSO). The 3-(4,5-dimethylthiazol-2-yl)-2,5-diphenyyltetrazolium bromide (MTT) assay (11465007001, Sigma-Aldrich) [22] was used to determine the cell viability according to the manufacturer's instructions. Briefly, MTT (10 μL) solution was added to each well and the plates were incubated for 4 h at 37 °C. After this period, the solubilizing buffer (10% SDS in 0.01 M HCl) was added to each well and the plates were incubated overnight at 37 °C. Absorbance (595 nm) measurements were determined for each well. Mean cell viability was calculated as a percentage of the mean vehicle control. At least three independent experiments in quadruplicate were performed.

### 3.4. Statistical analysis

Statistical analysis was conducted with the acquisition of the data represented as mean values and SEM (standard error of the means) of three independent experiments. The *t*-test (a student's statistical hypothesis test) was used to compare the two experimental frames and a value of $p < 0.5$ was accepted as statistically significant.

### 3.5. Density functional theory calculations

DFT calculations were performed to model the complexes **3a**, **3b** and **4**. The Guassian09 software package was used. The level of theory used for all calculations is B3LYP with the basis set 6-31 + G (d,p) for H, C, O, P, Cl and N atoms; while for Ru and Sn atoms the DGDZVP basis set was used. Geometry optimizations were calculated without any constraints. All the optimized geometries show non imaginary frequency. Energies and Natural Bond Order analyses were conducted on the optimized structures [33–36].

### 3.6. [RuCl($\eta^6$-$C_6H_5OCH_2CH_2OH$)($PPh_3$)($SnCl_3$)] (**3a**)

To a solution of **2a** (0.300 g, 0.524 mmol) in DCM (35 mL), anhydrous tin dichloride (0.109 g, 0.576 mmol) was added. The mixture was refluxed for 4.5 h. The solution was filtered, and the solvent removed in vacuo affording a dark red solid. Yield: 0.319 g (0.418 mmol, 79.8%). $^1$H NMR (300.1 MHz, DMSO-$d_6$, 296.2 K, ppm) $\delta$ 7.66–7.41 (m, 15H, P*Ph*$_3$), 6.40 (t, $^3J_{H,H} = 5.9$ Hz, 1H, $C_6H_5$), 6.09 (d, $^3J_{H,H} = 5.9$ Hz, 1H, $C_6H_5$), 5.94 (d, $^3J_{H,H} = 6.3$ Hz, 1H, $C_6H_5$), 5.59–5.54 (ps q, 1H, $C_6H_5$), 5.02 (broad s, 1H, O*H*), 4.24–4.17 (m, 1H, $C_6H_5$), 4.12–4.05 (m, 2H, $CH_2$O), 3.71 (broad s, 2H, $CH_2$OH). $^{13}$C{$^1$H} NMR (75.5 MHz, DMSO-$d_6$, 296.7 K, ppm) $\delta$ 143.4 (d, $C_{ipso}$, P*Ph*$_3$), 133.9 (d, $C_{meta}$, P*Ph*$_3$), 131.4 (d, $C_{para}$, P*Ph*$_3$), 129.3 (d, $C_{ortho}$, P*Ph*3), 77.9 (d, $^2J_{C,P} = 9.5$ Hz $C_{meta}$, $C_6H_5$), 72.2 (s, $C_{para}$, $C_6H_5$), 62.0 (s, $CH_2$O), 59.4 (s, $C_{ortho}$, $C_6H_5$) 55.4 (s, $CH_2$OH)($C^1$ of $C_6H_5$ ring not visible). $^{31}$P {$^1$H} NMR (121.5 MHz, DMSO-$d_6$, 298.2 K, ppm) $\delta$ 33.2 (s). FTIR 3078 (w, broad), 2959 (vvw), 1528 (m), 1464 (w), 1435 (m), 1265 (m, broad), 1092 (m), 1072–999 (w, broad), 910 (w, broad), 845 (w), 800 (w, broad), 746 (m), 692 (s), 667 (m) cm$^{-1}$. UV–Vis (nm) $\lambda_{max} = 376$. TGA: (Weight % decrease) 80 °C – 128.17 °C (3.847%), 128.17 °C – 237.71 (6.69%), 237.71 °C – 283.11 °C (6.52%), 283.11 °C – 321.01 °C (11.13%), 321.01 °C – 342.26 °C (14.22%), 342.26 °C – 375.16 °C (7.55%), 375.16 °C – 493.45 °C (5.70%). Melting point: 205 °C (dec.). $S^{\circ}_{20C}$ ($H_2O$) soluble, 0.03 mg/mL. ESI-MS 537.0331 (found), 537.0342 (calcd.)([M – $SnCl_3$]$^+$, 100%).

### 3.7. [RuCl($\eta^6$-$C_6H_5OCH_2CH_2OH$){P(OPh)$_3$}($SnCl_3$)] (**3b**)

To a solution of **2b** (0.300 g, 0.484 mmol) in DCM (35 mL), anhydrous tin dichloride (0.100 g, 0.532 mmol) was added. The mixture was refluxed for 4.5 h. The orange solution was filtered, and the solvent removed in vacuo affording a viscous red oil. The crude product was left to crystallize from a mixture of diethyl ether and DCM at −25 °C obtaining bright red crystals. Yield: 0.212 g (0.261 mmol, 54.0%). $^1$H NMR (300.1 MHz, $CDCl_3$, 296.2 K, ppm) $\delta$ 7.38–7.25 (m, 15H, P(O*Ph*)$_3$), 6.33 (t, $^xJ_{H,H} = 5.4$ Hz, 1H, $C_6H_5$), 5.76–5.74 (m, 1H, $C_6H_5$), 5.60–5.55 (m, 1H, $C_6H_5$), 4.52 (dd, $^3J_{H,H} = 2.03$ Hz, $^3J_{H,H} = 3.35$ Hz, 1H, O*H*), 4.16–4.10 (m, 1H, $C_6H_5$), 4.04–3.99 (m, 1H, $C_6H_5$), 3.93–3.83 (m, 2H, $CH_2$O), 3.71 (ps t, $^3J_{H,H} = 6.0$ Hz, 1H, $CH_{2A}$OH), 2.45 (t, 1H, $CH_{2B}$OH). $^{13}$C{$^1$H} NMR (75.5 MHz, DMSO-$d_6$, 295.2 K, ppm) $\delta$ 150.9 (d, $^2J_{C,P} = 10.0$ Hz, $C_{ipso}$, P(O*Ph*)$_3$), 130.0 (s, $C_{meta}$, P(O*Ph*)$_3$), 125.9 (s, $C_{para,}$ P(O*Ph*)$_3$), 121.7 (d, $^3J_{C,P} = 4.4$ Hz $C_{ortho}$, P(O*Ph*)$_3$), 94.6 (s, $C_{meta}$, $C_6H_5$), 92.2 (s, $C_{para}$, $C_6H_5$), 72.7 (s, $CH_2$O), 72.3 (s, $C_{ortho}$, $C_6H_5$), 60.4 (s, $CH_2$OH)($C^1$ of $C_6H_5$ ring not visible). $^{31}$P {$^1$H} NMR (121.5 MHz, $CDCl_3$, 296.2 K, ppm) $\delta$ 123.7 (s, $^2J_{119Sn,31P}$=896 Hz, $^2J_{117Sn,31P}$=849 Hz). $^{119}$Sn {$^1$H} NMR (111.8 MHz, $CDCl_3$, 298.2 K, ppm) $\delta$ −169.4 (d, $^2J_{119Sn,31P}$=974 Hz). FTIR 3000 (vw, broad), 1540 (vw), 1485 (vw), 1270 (vw, broad), 1190 (vw), 1150 (vw), 1080 (vw), 1020 (vw), 940 (vw), 900 (w, broad), 760 (w), 690 (w) cm$^{-1}$. UV–Vis (nm) $\lambda_{max} = 452$. TGA (Weight % decrease) 150 °C – 177.74 °C (3.27%), 177.74 °C – 225.24 (8.59%), 225.24 °C – 339.11 °C (18.40%), 399.11 °C – 404.81 °C (12.89%), 404.81 °C – 485.32 °C (14.81%). Melting point: 169 °C (dec.). $S^{\circ}_{20C}$ ($H_2O$) insoluble. ESI-MS 584.9194 (found), 585.0172 (calcd.) ([M – $SnCl_3$]$^+$, 27%).

## 4. Conclusion

Two novel half-sandwich Ru(II) compounds bearing trichlorostannyl ligands were successfully synthesized as potential anti-cancer agents: [RuCl($\eta^6$-$C_6H_5OCH_2CH_2OH$)($PPh_3$)($SnCl_3$)] (**3a**) and [RuCl($\eta^6$-$C_6H_5OCH_2CH_2OH$){P(OPh)$_3$}($SnCl_3$)] (**3b**) and their cytotoxicity compared with the related known complexes: [$RuCl_2$($\eta^6$-$C_6H_5OCH_2CH_2OH$)($PPh_3$)](**2a**), [$RuCl_2$($\eta^6$-$C_6H_5OCH_2$-$CH_2OH$){P(OPh)$_3$}] (**2b**), [$RuCl_2$($\eta^6$-$C_6H_5OCH_2CH_2OH$){P(OMe)$_3$}] (**2c**), and [$RuCl_2$($\eta^6$-$C_6H_5OCH_2CH_2OH$)(PTA)] (**4**). Both new complexes were characterized using IR-spectroscopy, multinuclear NMR spectroscopy, UV–Vis spectroscopy and TGA as well as high resolution ESI-MS. Complex **3b** was also characterized by single crystal X-ray diffraction analysis. The aim to increase the bioavailability *via* increasing hydrophilicity was gauged using a simple water solubility test finding the complexes **3a** and **4** to be water soluble, while **3b** was insoluble. Compounds **2(a–c), 3(a)** and **4** is somewhat cytotoxic to MCF-7 breast cancer cells at the concentrations tested. The low cytotoxicity of compound **3b** is likely due to the only partial solubility of the compound in DMSO, thus offsetting the compound's capability to induce cellular apoptosis. Hence in this study the complexes **2a** and **2b** are *more* cytotoxic than their trichlorotin analogues **3a** and **3b**, suggesting that despite attachment of a hydrophilic substituent to the $\eta^6$-arene ring, insolubility caused by the trichlorostannyl ligand still might impede cytotoxicity of the latter. An investigation into the solubility of these

compounds in a synthetic buffer like that of the human body may provide more accurate results.

## Acknowledgements

The authors wish to thank the Maastricht Science Programme (MSP) and Maastricht University for financial support of this research. The University of Cape Town acknowledges financial support from the National Research Foundation (NRF), Cancer Association of South Africa (CANSA) and the South African Medical Research Council (SAMRC). We would like to thank Dr. Jade Peres and Mrs. Alexis Neumann-Mufweba who kindly assisted with the cell culture and cytotoxicity assays described in this study.

## Appendix A. Supplementary data

Supplementary data related to this article can be found at https://doi.org/10.1016/j.jorganchem.2019.04.002.

## References

[1] K.R. Harrap, M. Jones, C.R. Wilkinson, H.M. Clink, S. Sparrow, B.C. Mitchley, S. Clarke, A. Veasey, Antitumor, toxic and biochemical properties of cisplatin and eight other platinum complexes. Cisplatin, Elsevier, 1980, pp. 193–212.
[2] A.W. Prestayko, J. D'aoust, B. Issell, S. Crooke, Cancer Treat Rev. 6 (1979) 17–39.
[3] G. Süss-Fink, Dalton Trans. 39 (2010) 1673–1688.
[4] I. Kostova, Curr. Med. Chem. 13 (2006) 1085–1107.
[5] P.C. Bruijnincx, P.J. Sadler, Curr. Opin. Chem. Biol. 12 (2008) 197–206.
[6] C.S. Allardyce, P.J. Dyson, Platin. Met. Rev. 45 (2001) 62–69.
[7] S. Thota, D.A. Rodrigues, D.C. Crans, E.J. Barreiro, J. Med. Chem. 61 (2018) 5805–5821.
[8] L. Zeng, P. Gupta, Y. Chen, E. Wang, L. Ji, H. Chao, Z.-S. Chen, Chem. Soc. Rev. 46 (2017) 5771–5804.
[9] L. Guo, G. Lv, L. Qiu, H. Yang, L. Zhang, H. Yu, M. Zou, J. Lin, Eur. J. Pharmacol. 786 (2016) 60–71.
[10] J. Reedijk, Platin. Met. Rev. 52 (2008) 2–11.
[11] B.S. Murray, M.V. Babak, C.G. Hartinger, P.J. Dyson, Coord. Chem. Rev. 306 (2016) 86–114.
[12] A. Weiss, X. Ding, J.R. Van Beijnum, I. Wong, T.J. Wong, R.H. Berndsen, O. Dormond, M. Dallinga, L. Shen, R.O. Schlingemann, Angiogenesis 18 (2015) 233–244.
[13] A.A. Nazarov, S.M. Meier, O. Zava, Y.N. Nosova, E.R. Milaeva, C.G. Hartinger, P.J. Dyson, Dalton Trans. 44 (2015) 3614–3623.
[14] A. Bergamo, G. Sava, Dalton Trans. (2007) 1267–1272.
[15] G. Sava, S. Zorzet, C. Turrin, F. Vita, M. Soranzo, G. Zabucchi, M. Cocchietto, A. Bergamo, S. DiGiovine, G. Pezzoni, Clin. Cancer Res. 9 (2003) 1898–1905.
[16] M. Gielen, Coord. Chem. Rev. 151 (1996) 41–51.
[17] M. Gras, B. Therrien, G. Süss-Fink, A. Casini, F. Edafe, P.J. Dyson, J. Organomet. Chem. 695 (2010) 1119–1125.
[18] O. Renier, C. Deacon-Price, J.E. Peters, K. Nurekeyeva, C. Russon, S. Dyson, S. Ngubane, J. Baumgartner, P.J. Dyson, T. Riedel, Inorganics 5 (2017) 44.
[19] C. Deacon-Price, D. Romano, T. Riedel, P.J. Dyson, B. Blom, Inorg. Chim. Acta 484 (2019) 513–520.
[20] B. Lastra-Barreira, J. Diez, P. Crochet, Green Chem. 11 (2009) 1681–1686.
[21] L.C. Matsinha, P. Malatji, A.T. Hutton, G.A. Venter, S.F. Mapolie, G.S. Smith, Eur. J. Inorg. Chem. (2013) (2013) 4318–4328.
[22] J. Carmichael, W.G. DeGraff, A.F. Gazdar, J.D. Minna, J.B. Mitchell, Cancer Res. 47 (1987) 936–942.
[23] J.O. Suberu, I. Romero-Canelón, N. Sullivan, A.A. Lapkin, G.C. Barker, ChemMedChem 9 (2014) 2791–2797.
[24] T.S. Morais, F. Santos, L. Corte-Real, F. Marques, M.P. Robalo, P.J.A. Madeira, M.H. Garcia, J. Inorg. Biochem. 122 (2013) 8–17.
[25] J. Soleimannejad, C. White, Organometallics 24 (2005) 2538–2541.
[26] SAINTPLUS, Software Reference Manual, Bruker-AXS, Madison, WI, 1997-2003, Version 6.45.
[27] G.M. Sheldrick, SADABS. Version 2.10, Bruker AXS Inc., Madison, WI, 2003.
[28] R.H. Blessing, Acta Crystallogr. A 51 (1995) 33–38.
[29] G.M. Sheldrick, Acta Crystallogr. C: Struct. Chem. 71 (2015) 3–8.
[30] G.M. Sheldrick, Acta Crystallogr. A: Foundations of Crystallography 64 (2008) 112–122.
[31] L.J. Farrugia, J. Appl. Crystallogr. 45 (2012) 849–854.
[32] POVRAY 3.6, Persistence of Vision Pty. Ltd., Williamstown, Victoria, Australia, 2004. Available online: http://www.povray.org/download/. (Accessed 9 July 2008).
[33] A.D. Becke, J. Chem. Phys. 98 (1993) 5648–5652.
[34] C. Lee, W. Yang, R.G. Parr, Phys. Rev. B 37 (1988) 785.
[35] B. Miehlich, A. Savin, H. Stoll, H. Preuss, Chem. Phys. Lett. 157 (1989) 200–206.
[36] R.E. Gaussian 09, M.J. Frisch, G.W. Trucks, H.B. Schlegel, G.E. Scuseria, M.A. Robb, J.R. Cheeseman, J.A. Montgomery Jr., T. Vreven, K.N. Kudin, J.C. Burant, J.M. Millam, S.S. Iyengar, J. Tomasi, V. Barone, B. Mennucci, M. Cossi, G. Scalmani, N. Rega, G.A. Petersson, H. Nakatsuji, M. Hada, M. Ehara, K. Toyota, R. Fukuda, J. Hasegawa, M. Ishida, T. Nakajima, Y. Honda, O. Kitao, H. Nakai, M. Klene, X. Li, J.E. Knox, H.P. Hratchian, J.B. Cross, V. Bakken, C. Adamo, J. Jaramillo, R. Gomperts, R.E. Stratmann, O. Yazyev, A.J. Austin, R. Cammi, C. Pomelli, J.W. Ochterski, P.Y. Ayala, K. Morokuma, G.A. Voth, P. Salvador, J.J. Dannenberg, V.G. Zakrzewski, S. Dapprich, A.D. Daniels, M.C. Strain, O. Farkas, D.K. Malick, A.D. Rabuck, K. Raghavachari, J.B. Foresman, J.V. Ortiz, Q. Cui, A.G. Baboul, S. Clifford, J. Cioslowski, B.B. Stefanov, G. Liu, A. Liashenko, P. Piskorz, I. Komaromi, R.L. Martin, D.J. Fox, T. Keith, M.A. Al-Laham, C.Y. Peng, A. Nanayakkara, M. Challacombe, P.M.W. Gill, B. Johnson, W. Chen, M.W. Wong, C. Gonzalez, J.A. Pople, Gaussian, Inc., Wallingford CT, 2004.